Infrared Chemiluminescence Study of the Reactions of Hydroxyl Radicals with Formaldehyde and Formyl Radicals with H, OH, NO, and NO_2

N. I. Butkovskaya

Institute of Chemical Physics, Russian Academy of Sciences, 117334 Moscow, Russian Federation

D. W. Setser*

Department of Chemistry, Kansas State University, Manhattan, Kansas 66506

Received: June 30, 1998; In Final Form: September 24, 1998

The infrared chemiluminescence in the 1800−3900 cm^{-1} range was observed from vibrationally excited products generated by the reactions of OH and OD with H_2CO in a fast flow reactor with 0.5−1.0 Torr of Ar carrier gas. Computer simulation of the emission spectra from H_2O and HOD molecules generated by the primary reaction gave an inverted vibrational distribution in the ν_3(O−H) stretching mode of HOD, with a maximum population in $\upsilon_3 = 1$; the distribution for the ν_1 and ν_3 stretch modes of H_2O was similar. The vibrational energy disposal to H_2O and HOD was $\langle f_v \rangle = 0.54-0.56$ with 63% in the newly formed OH bond and 34% in the bending mode. This vibrational distribution is characteristic for a direct abstraction mechanism. The excitation in the bending mode exceeds that from OH reactions with hydrocarbons (<20%), but it is similar to that from the reaction of OH with dimethyl sulfide and HBr. By adjustment of the reaction conditions, infrared emission could be observed from secondary reactions of HCO radical with NO_2, NO, OH, and H atoms. The vibrational distributions of H_2O and HOD from the primary reaction plus the vibrational distributions of CO_2 and CO from the NO_2 + HCO reaction, HNO from the NO + HCO reaction, H_2O and CO from the OH + HCO reaction, and CO from the H + HCO reaction were analyzed using information theory. The results support an addition mechanism followed by unimolecular decomposition for the HCO radical reactions. The vibrational of H_2O distribution from OH + HCO is especially noteworthy, since it can be used to distinguish between direct abstraction vs recombination followed by the decomposition of HCOOH.

1. Introduction

Formaldehyde and formyl radical are important intermediates in the oxidation of hydrocarbons. Understanding their key roles in combustion and atmospheric chemistry requires a knowledge of their reactivity and detailed reaction mechanisms so that the complex oxidation and pyrolysis of organic compounds can be modeled. All the title reactions have been investigated previously, their rate constants have been determined, and many mechanistic and dynamical details are known.[1−13] The aim of this work is to get further insight into the dynamics of the OH + CH_2O reaction and to study the secondary reactions of the HCO radical with NO_2, NO, OH, and H atoms by observing vibrational distributions of the products. The experimental technique is the observation of infrared chemiluminescence from a fast-flow reactor operating at ∼1 Torr of Ar and room temperature.

In recent work we have determined the vibrational excitation of isotopic water molecules formed in the reactions of OH(OD) radical with a number of small molecules, including HBr,[14] HI and GeH_4,[15] HCl, *n*-butane, and cyclohexane,[16] H_2S, CH_3SH, and $(CH_3)_2S$.[17] The assigned vibrational distributions are for the collisionally equilibrated reservoirs of nearly resonant modes, namely, the ν_1 and ν_3 modes of H_2O, and the ν_1 and $2\nu_2$ modes of HOD, plus the bending mode, ν_2, for H_2O and the O−H stretch, ν_3, of HOD. These data uniquely identify the total vibrational energy and the energy released to the newly formed O−H bond of HOD and into the bending mode of H_2O. Comparison with thoroughly studied atom−diatom reactions,[18] especially the reactions of isoelectronic F atoms, showed that the dynamics found for **H** + **L** − **H** three-body reactions have many features in common with H atom abstraction reactions by OH(OD) radicals. In particular, the H_2O and HOD vibrational distributions extend to the thermochemical energy limit with inverted populations in the stretching mode for the HBr, hydrocarbon, H_2S, and $(CH_3)_2S$ reactions. Also, an inverse correlation exists between the excitation energy in the bending and stretching modes.

In the present study, the infrared chemiluminescent spectra of H_2O and HOD were measured and analyzed from the reactions of OH and OD radicals with formaldehyde at 298 K.

$$OH + H_2CO \rightarrow H_2O + HCO \quad (1)$$

$$OD + H_2CO \rightarrow HOD + HCO \quad (1D)$$

These data are representative for reactions with carbonyl compounds, which is a different class of reagent from previously investigated reactions.[14−17] The reactions occurred in a fast-flow reactor which was viewed by a Fourier transform infrared spectrometer. The fast H(D) + NO_2 → OH + NO reaction was used as a source of OH(OD) radicals. The vibrational distributions for the primary H_2O(HOD) products were obtained under conditions that were free of secondary reactions giving water and vibrational relaxation. These nascent distributions are compared to H_2O and HOD distributions from other reactant molecules with an emphasis on the ratio of the stretch-to-bend excitation.

10.1021/jp982810r CCC: $15.00
Published on Web 11/10/1998

TABLE 1: Thermodynamical and Kinetic Data for OH + H_2CO and Secondary Reactions of HCO

reaction	k(298 K) ($cm^3\ s^{-1}$)	E_a (kcal mol^{-1})	$-\Delta H°_0$ (kcal mol^{-1})	$\langle E_{av}\rangle$ (kcal mol^{-1})	ref
1. $OH + H_2CO \rightarrow H_2O + HCO$	$(9.6 \pm 0.2) \times 10^{-12}$	-0.05 ± 0.30	30.8	33.2	1
2. $NO_2 + HCO \rightarrow$ products	$(5.6 \pm 0.9) \times 10^{-11}$	-0.43 ± 0.48			9
$\rightarrow HONO + CO$			64.0	66.7	
$\rightarrow HO + NO + CO$			12.5	14.3	
$\rightarrow H + NO + CO_2$			40.2	42.0	
3. $NO + HCO \rightarrow HNO + CO$	$(1.2 \pm 0.1) \times 10^{-11}$	0	32.7	35.1	12
4. $OH + HCO \rightarrow$ products	1.8×10^{-10}	0			2
	5×10^{-11}				3
$\rightarrow H_2O + CO$			104.1	106.5	
$\rightarrow H_2 + CO_2$			113.9	116.3	
5. $H + HCO \rightarrow H_2 + CO$	$(2.0 \pm 0.2) \times 10^{-10}$	0	89.3	91.1	3
	$(1.4 \pm 0.4) \times 10^{-10}$	-0.75			4

The energy available to the products of reaction 1 can be obtained from the equation $\langle E_{av}\rangle = -\Delta H°_0 + 4RT + E_a$, where E_a is the activation energy and $\Delta H°_0$ is the reaction enthalpy. The thermodynamical and kinetic data for reactions involved in the study are presented in Table 1. The enthalpy of reaction 1 was calculated from the recent data for the bond energies[19,20] $D_0(H-CHO) = 87.3$ kcal mol^{-1} and $D_0(H-OH) = 118.08$ kcal mol^{-1}, which gives $\Delta H°_0 = -30.8$ kcal mol^{-1}. The available energy is 33.2 kcal mol^{-1}, which is sufficient to excite up to three stretching quanta and up to six bending quanta in the water molecule.

The $H/NO_2/H_2CO$ prereaction system also proved to be a convenient way to obtain infrared chemiluminescence from the secondary reactions of HCO radical with NO_2, NO, and OH, and H atoms (these reactions will be identified as reactions 2, 3, 4, and 5, respectively). The secondary reactions of HCO radical are highly exothermic (see Table 1) due to the very weak H−C bond[19] in formyl radical, $D_0(H-CO) = 15$ kcal mol^{-1}, and high vibrational excitation of the products could be possible. The principal question for the H and OH + HCO reactions is whether they proceed by a direct H-atom abstraction process or by radical−radical recombination followed by unimolecular decomposition to give equivalent chemical products. Even though the chemical identity of the products are the same at low pressures, the vibrational distributions of the products are expected to be very different for the two mechanisms. The H_2O-(HOD) products of the OH(OD) + HCO secondary reactions were analyzed using the relative intensities between the observed H_2O(HOD) and CO emission to separate the H_2O(HOD) primary and secondary emission. The H_2O(HOD) vibrational distributions from the secondary reaction are not even as highly excited as those from the primary reaction, which identifies an addition−elimination mechanism for this OH + HCO reaction. The emissions from other secondary products, CO_2 from the NO_2 + HCO reaction, HNO from the NO + HCO reaction,[21] and CO from the reactions of HCO with NO_2, OH, and H, were also analyzed by computer simulation, and the distributions are compared with statistical distributions using the method of surprisal analysis.

2. Experimental Methods

2.1. Experimental Setup. In the present work, the infrared chemiluminescence (Figure 1) from vibrationally excited H_2O, CO_2, CO, and HNO molecules was recorded by a Fourier transform infrared spectrometer (BIORAD) from a fast-flow reactor at 298 K. The spectral resolution was 1 cm^{-1}. The response of the liquid N_2 cooled InSb detector was calibrated with a standard blackbody source. The entire optical system was flushed continuously with air that had been passed through a commercial unit that removed H_2O and CO_2. The total

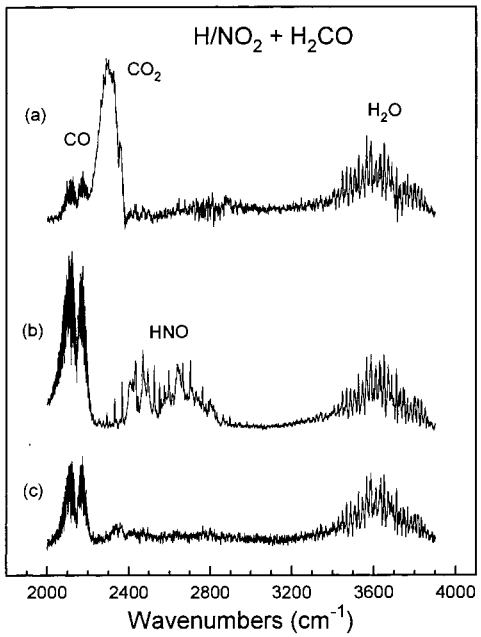

Figure 1. Raw infrared emission spectra produced in the H/NO_2 + H_2CO chemical system at 1 Torr ($\Delta t = 0.5$ ms): (a) $[NO_2] = 1.8 \times 10^{14}$, $[H_2] = 2.3 \times 10^{13}$ molecules cm^{-3}; (b) $[NO_2] = 8.0 \times 10^{13}$, $[H_2] = 4.2 \times 10^{13}$ molecules cm^{-3}; (c) $[NO_2] = 1.8 \times 10^{13}$, $[H_2] = 4.0 \times 10^{13}$ molecules cm^{-3}. Each spectrum is normalized to the intensity of the strongest H_2O peak.

pressure in the 4 cm diameter reactor was 0.5−1.0 Torr using Ar as a carrier gas; the corresponding reaction time (Δt) was 0.22−0.45 ms. The Ar, H_2, and NO_2 were metered to the reactor using standard methods. Commercial tank grade Ar was passed in succession through three molecular sieve filled traps cooled by either an acetone/dry ice mixture or liquid nitrogen to remove impurities. Tank grade H_2 and D_2 were used without purification. Additional experimental details can be found in earlier papers.[14,22]

The OH (or OD) radicals were produced 30 cm upstream of the observation window (NaCl) via the fast H(D) + $NO_2 \rightarrow$ OH(OD) + NO reaction, which also was the source of NO molecules. The H atoms were generated by a microwave discharge in a $H_2(D_2)$/Ar mixture, the degree of the dissociation[22] was ~50% for H_2 concentrations $\leq 2 \times 10^{13}$ molecules cm^{-3}. For study of the primary reaction, the concentration of H atoms was in the range of $(1-3) \times 10^{12}$ molecules cm^{-3}. Formaldehyde was introduced into the reactor through the injector located 3.5 cm upstream of the observation window. The H_2-CO vapor was carried by an argon flow that was passed over a sample of paraformaldehyde powder (Fisher Scientific) heated to 110 C. Typical H_2CO concentrations were about 5×10^{13}

molecules cm^{-3}, as determined by the rate of powder consumption. The paraformaldehyde sample was purified by pumping under vacuum at 40−50 °C for 2 days. The absence of water concentration in the sample was verified by the addition of F atoms to the reactor: the F + CH_2O and F + H_2O reactions give significantly different HF spectra.[18a,c] The OH or NO emission from the H + NO_2 reaction was not observed with the discharge running in the absence of formaldehyde, which proves that all the H atoms were converted to hydroxyl radicals upstream in the reactor.

The typical concentration of NO_2 for study of the primary and NO_2 + HCO secondary reactions was about 1×10^{14} molecules cm^{-3}. The best conditions to observe the secondary reactions of OH and NO were $[NO_2] \approx [H_2] \approx 3 \times 10^{13}$ molecules cm^{-3}. To identify emission from the H + HCO secondary reaction, an excess H atom concentrations was needed, and the H_2 concentration was elevated to $\approx 5 \times 10^{13}$ molecules cm^{-3}.

2.2. Modeling of Spectra. *H_2O and HOD.* As in our previous works,[14−17] simulation of the H_2O and HOD spectra was based on using the line intensities for the (001), (100), and (020) fundamental bands in absorption from the HITRAN database.[23] Calculation of the corresponding emission bands was made using the exact line positions for H_2O transitions with an assumed 300 K Boltzmann rotational distribution. The line positions of transitions from higher levels were obtained as difference in vibrational−rotational energy levels as outlined in ref 15. Adjustments for some of the previously calculated[15] line positions of H_2O bands with high υ_2 numbers were made using new data for the band origins. The most serious corrections, +11.0 and −4.2 cm^{-1}, are for the (051) and (061) bands, respectively, from the accurately determined band centers from the transition frequencies of the (051)−(040) and (061)−(050) combination bands.[24] The rotational line intensities were taken to be the same as for the fundamental bands; the *adjusted* harmonic oscillator approximation, weighted by ν^3, was used to obtain the relative Einstein coefficients for the vibrational states. The appendix of ref 15 should be consulted for details about the Einstein coefficients.

The similar energies of the symmetric and antisymmetric stretching vibrational levels of H_2O lead to fast collisional equilibration between these modes, so that only equilibrium population of $\upsilon_{1,3} = \upsilon_1 + \upsilon_3$ stretching levels can be assigned in our experiments. The υ_2 distribution can be assigned from the emission spectra for each $\upsilon_{1,3}$ level. The nascent υ_3 population of HOD can be obtained separately from reaction 1D, because the frequencies of the two normal stretching modes of HOD are quite different. However, Fermi resonance between the ν_1 and $2\nu_2$ modes of HOD will facilitate the rapid establishment of equilibrium between the coupled ν_1 and $2\nu_2$ sets of levels. Accordingly, the obtained distributions are for the $\nu_{1,2}$ equilibrium states denoted by the equivalent number of bending quanta $\nu_{1,2}$, i.e., $\upsilon_{1,2} = 4$, $\upsilon_3 = 1$ denotes the group of 041, 121, and 201 states.

The least-squares fitting method employed to obtain the best simulation of a spectrum was fully described in earlier papers,[14−16] and the uncertainties of the vibrational populations associated with the best simulation were discussed in ref 17. The least-squares best-fit parameter, $Q = \sum_i [s_i - \sum_k (p_k b_{ki})]^2$, where s_i is the data point and b_{ki} is the ith element of the band from the k-state with the population parameter p_k, was typically $< 7 \times 10^5$ for spectra consisting of $N = 1452$ points and normalized to the maximum peak value of 320 units. The estimated standard deviations are about 7% for the populations in the $P_{1,3}(1)$ and $P_{1,3}(2)$ states of H_2O and about 3% for the populations in the $P_3(1)$ and $P_3(2)$ states of HOD. Accordingly, the $P(1)/P(2)$ ratios are known to within −10% and −5% for H_2O and HOD, respectively. The $P(0)/P(1)$ are somewhat less certain, vide infra, but the use of data for both H_2O and HOD reduces the uncertainty for the relative populations in $\upsilon_3 = 0$ and $\upsilon_{1,3} = 0$ states. Uncertainties for the weakly populated $\upsilon_{1,3} = 3$ and $\upsilon_3 = 3$ states are of the order of 80% for $P_{1,3}(3)$ and 60% for $P_3(3)$.

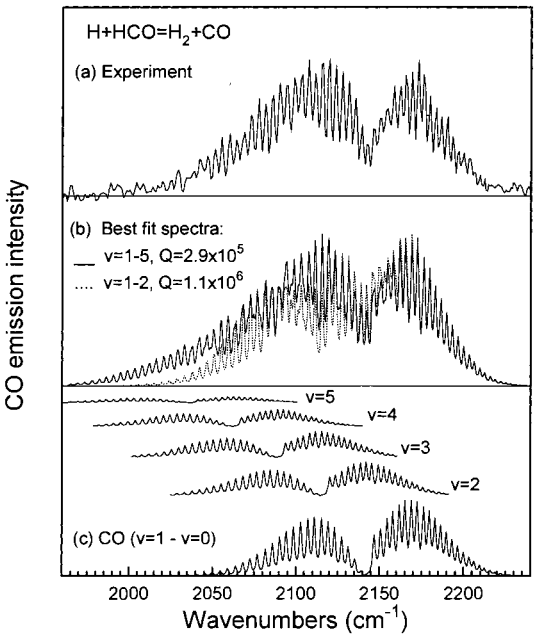

Figure 2. Illustration of the simulation of the CO emission spectrum from the H + HCO reaction: (a) experimental spectrum, (b) two examples of simulated spectra showing the need to include ≥3 levels, and (c) the individual components in the preferred distribution.

CO. The observed CO emission was fitted as a superposition of $\Delta\upsilon = -1$ transitions from the fundamental and hot bands. The P- and R-branch line positions were calculated using the conventional expressions for the vibrational and rotational energy levels with the spectroscopic molecular constants ω_e, $\omega_e x_e$, $\omega_e y_e$, B_e, α_e, and D_e from ref 25. The relative intensities were calculated according to eq I

$$I = c_{em} \nu^3 (2J + 1) \exp(-W_R/kT) F_{vJ} \qquad \text{(I)}$$

where c_{em} is a common constant for all the transitions, ν is the transition frequency, and F_{vJ} is the oscillator strengths for CO rovibrational transitions.[26a] The calculated $\Delta\upsilon = -1$ bands from $\upsilon = 1$ to 5 for a 300 K rotational distribution are shown in Figure 2c as constituents of the CO(υ) model spectra for the H + HCO reaction. The R-branch lines in the 1−0 emission band are not significantly overlapped and comparison of the computed and calculated spectra shows that the rotational distribution must be 300 K, because the experimental R-branch lines do not extend beyond 2220 cm^{-1}. At a pressure of 0.5 Torr of Ar for a time of 0.3 ms, rotational relaxation is expected. A typical experimental spectrum is shown in Figure 2a. The contributions to the spectrum from different υ levels were obtained by the least-squares simulation of the observed CO spectra. The standard deviation of the vibrational populations can be evaluated through the error analysis described for simulation of the water spectra.[14,17] The least-squares estimators for CO spectra were typically $Q \approx 2.7 \times 10^5$ for spectra consisting of 540 points.

The standard deviation of CO vibrational populations from the modeling does not exceed 2%, 4%, 5%, 8%, and 23% for the $v = 1$, 2, 3, 4, and 5 levels, respectively. Taking into account the noise level, the uncertainties in the population ratios $P(2)/P(1)$, $P(3)/P(2)$, and $P(4)/P(3)$ were estimated to be 11%, 18% and 26%, respectively, for the spectrum in Figure 2c. The contribution of the $v = 5$ band is within the noise level, and the $v = 5$ component of the distribution has 70% uncertainty.

The question of the possible vibrational relaxation of CO(v) by NO_2, OH, or H atoms needs to be considered. The OH(v=1) + CO quenching reaction has a rate constant of only 1.0×10^{-12} cm^3 s^{-1} at 300 K[27] and the relaxation rate for CO(v) + OH should not be any faster. Hence, the OH concentration in the reactor will not cause relaxation of CO(v). The relaxation of CO(v) by NO_2 also should be slow.[28] The CO + H potential surface has a barrier of 2−3 kcal mol^{-1},[29] so the association rate of H + CO(v) to give HCO also should be slow at room temperature. Thus, the distributions assigned to CO(v) emission spectra should correspond to nascent distributions.

CO_2. Simulation of the CO_2 spectra has been already described in our report of the unimolecular decomposition of acetic acid.[30] The observed emission was modeled as the overlap of $\Delta v_3 = -1$ transitions from (v_1, v_2^l, v_3)−(v_1, v_2^l, v_3 − 1) combination bands with the rigid-rotor approximation for vibrational−rotational line intensities. The band centers were calculated according to the conventional formula for the vibrational levels of a linear molecule with a doubly degenerate bending vibration, v_2. The frequencies ω_i, anharmonicity coefficients x_{ik}, and g_{22} coefficient were taken from ref 31. As already noted,[30] simulation of the CO_2 spectra does not allow transitions from the $v_3 = 1$ level to be distinguished from those originating from higher v_3 states in the presence of bending excitation because the similar $x_{33} = -12.47$ and $x_{23} = -12.37$ cm^{-1} values lead to overlap of the (v_1, v_2, v_3) and (v_1, $v_2 - 2$, $v_3 + 1$) bands. Our calculations were made just for the $v_3 = 1$ state plus bending excitation, and the actual v_3 distribution may be somewhat broader.

HNO. The emission in the 2250−2900 cm^{-1} range was assigned to the HNO molecule in a preliminary report.[21] The two main bands of the spectrum were perfectly predicted by a simulation using the HNO spectroscopic constants[32] with intensities given by the direction-cosine matrix elements for a prolate symmetric top. The experimentally assigned $2\nu_1 - \nu_1$ band origin, 2452 cm^{-1}, and anharmonicity coefficient, $x_{11} = -116$ cm^{-1}, confirmed the ab initio calculated value $x_{11} = -113.4$ cm^{-1}.[33]

3. Experimental Results

3.1. Identification of Chemical Reactions in the H/NO_2 + H_2CO System. The raw emission spectra from the H/NO_2 + H_2CO reaction system are shown in Figure 1. The spectra were measured at a total pressure of 1 Torr ($\Delta t = 0.45$ ms) for different initial NO_2 and H_2 concentrations in the reactor. The spectra, which are normalized to the most intense H_2O peak, were acquired with 1024 scans of the spectrometer. All spectra contain H_2O emission in the 3200−3900 cm^{-1} range from the primary reaction 1, which consists mainly of $\Delta v_3 = -1$ transitions. In addition to H_2O emission, intense chemiluminescence was observed in the 2000−2800 cm^{-1} range, from the secondary reactions of formyl radical with NO_2, NO, OH, and H. The dominant secondary reaction depends on the relative concentrations of the reactants, and the three following cases were distinguished:

A. [NO_2] ≫ [H_2] (Figure 1a). In large excess of NO_2 the only important secondary reaction is reaction 2, with an overall rate constant $k_2 = 5.7 \times 10^{-11}$ cm^3 s^{-1}.[9]

$$NO_2 + HCO \rightarrow HONO + CO \quad (2a)$$

$$\rightarrow OH + NO + CO \quad (2a')$$

$$\rightarrow HCOO + NO \rightarrow H + CO_2 + NO \quad (2b)$$

$$\rightarrow HNO + CO_2 \quad (2c)$$

Figure 1a corresponds to [NO_2] = 1.8×10^{14} and [H_2] = 2.3×10^{13} molecules cm^{-3}. The observed products are H_2O from the primary reaction and CO and CO_2 in the 2000−2400 cm^{-1} range. Since HNO is not observed, channel 2c is not important and the observed CO_2 emission is entirely due to channel 2b. This conclusion agrees with recent claims[9,10] for the product branching ratios for reaction 2. However, the relative importance of (2a), (2a′), and (2b) is still debated, and this question will be examined in the Discussion section after our data are analyzed.

B. [NO_2] ≈ [H_2]. At comparable concentrations, [NO_2] = 8.0×10^{13} and [H_2] = 4.2×10^{13} molecules cm^{-3}, emission in the 2400−2900 cm^{-1} range becomes observable (Figure 1b). This emission belongs to the $\Delta v_1 = -1$ transitions of HNO molecule[21] produced in reaction 3 with a rate constant $k_3 = 1.2 \times 10^{-11}$ cm^3 s^{-1}.[12]

$$NO + HCO \rightarrow HNO + CO \quad (3)$$

For these conditions, [NO] ≈ [OH] > [NO_2] or [H], the very fast reaction with OH radical with a rate constant $k_4 = 1.8 \times 10^{-10}$ cm^3 s^{-1} [2] also occurs

$$OH + HCO \rightarrow H_2O + CO \quad (4)$$

which can result in a substantial growth of CO emission plus an additional contribution to the H_2O spectrum.

C. [H_2] > [NO_2]. For an excess of hydrogen, the only important secondary process is reaction 5.

$$H + HCO \rightarrow H_2 + CO \quad (5)$$

This reaction is so fast, $k_5 = 2 \times 10^{-10}$ cm^3 s^{-1},[3] that a 2-fold excess of hydrogen is sufficient to inhibit all other secondary reactions, and the only observable products are water from the primary reaction and CO from (5), as can be seen from the spectrum in Figure 1c.

Much weaker signals with characteristic central peaks were observed in the 1840−1960 cm^{-1} region for certain conditions (Figure 3). At 0.5 Torr and [NO_2]/[H], the central peak is positioned around 1867 cm^{-1} and can be assigned as a Q-branch of the ν_3 band of HCO (C−O vibration).[34] This branch is shown in Figure 3b for 0.5 Torr pressure and [NO_2] = 2.8×10^{13} and [H_2] = 1.8×10^{13} molecules cm^{-3}. At elevated pressure (>1 Torr) with excess NO_2, the signal changes its structure as shown in Figure 3a. The latter spectrum was attributed to the 1−0 band of NO($^2\Pi$) with the Q-branch head at ≈1876 cm^{-1}.[25] The R-branch of NO with rotational lines separated by $2B_e \approx 3.7$ cm^{-1} also is evident. The NO emission probably is from reaction 2.

3.2. Vibrational Distribution from the Primary OH(OD) + H_2CO Reaction. Since neither reaction 2 nor reaction 5 produces H_2O, experimental conditions of excess [NO_2] or excess [H] can be used to obtain spectra from just the primary

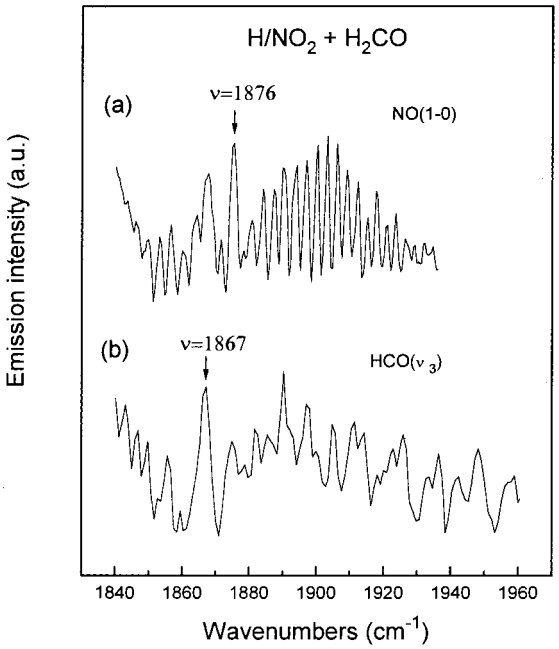

Figure 3. Raw spectra in the 1800−1940 cm^{-1} range observed from the $H/NO_2 + CH_2O$ system: (a) NO(1−0) at 1.0 Torr ($\Delta t = 0.5$ ms) with $[NO_2] = 1.8 \times 10^{14}$, $[H_2] = 4.0 \times 10^{13}$ molecules cm^{-3}, and (b) HCO(ν_3) at 0.5 Torr with $[NO_2] = 2.8 \times 10^{13}$, $[H_2] = 1.8 \times 10^{13}$ molecules cm^{-3}.

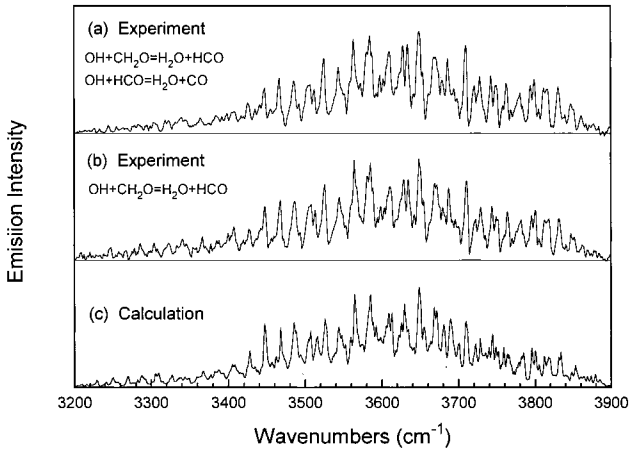

Figure 4. Spectra of H_2O, adjusted for wavelength response, measured at 0.5 Torr ($\Delta t = 0.25$ ms): (a) $[NO_2] = 2.7 \times 10^{13}$ and $[H_2] = 1.8 \times 10^{13}$ molecules cm^{-3} (this spectrum includes emission from both OH + H_2CO and OH + HCO reactions) and (b) with $[NO_2] = 7.2 \times 10^{13}$ and $[H_2] = 1.2 \times 10^{12}$ molecules cm^{-3} (this spectrum is for just the OH + H_2CO reaction). The calculated spectrum (c) corresponds to the vibrational distribution in Table 2 for H_2O from just the primary reaction.

reaction. A response corrected H_2O spectrum for $[NO_2] = 7.2 \times 10^{13}$ and $[H_2] = 1.2 \times 10^{12}$ molecules cm^{-3}, which is the highest $[NO_2]/[H_2]$ ratio used in the experiments is presented in Figure 4b. The H_2O and HOD spectra to be fitted were acquired for 0.5 Torr and a residence time of 0.25 ms. For this residence time, Ar pressure and reactant concentrations, the vibrational relaxation of H_2O and HOD have been shown to be negligible by specific experimental tests.[15−17] The bottom section of Figure 4 shows the best-fit calculated spectrum, corresponding to the vibrational distribution in Table 2. The stretching distribution $P_{1,3}(\upsilon_{1,3})$ for H_2O, which is a summation over the bending quantum number υ_2, decreases for the $\upsilon_{1,3} = 1-3$ states, with $P_{1,3}(2)/P_{1,3}(1) = 0.6$. The population in $\upsilon_{1,3} = 0$ was estimated with the help of a linear surprisal analysis

TABLE 2: Vibrational Distribution of H_2O from the Reaction of OH with CH_2O

	υ_2								
$\upsilon_{1,3}$[a]	0	1	2	3	4	≥5	$P_{1,3}$[b]	$P_{1,3}$[c]	$P°_{1,3}$
				$[NO_2] \gg [H_2]$[e]					
0								21.2	53.7
1	13.6	16.9	14.0	10.8	5.0		60.3	47.5	35.5
2	15.5	11.9	6.6				33.9	26.7	10.4
3	5.8						5.8	4.6	0.35
P_2[d]	32.0	28.3	20.9	12.1	5.6	1.1			
$P°_2$	43.1	26.2	15.6	8.4	4.2	2.5			
				$[NO_2] \ll [H_2]$[e]					
0								21.2	53.7
1	9.9	17.2	12.7	10.4	7.0		57.2	45.1	35.5
2	13.4	13.5	8.7				35.5	28.0	10.4
3	7.3						7.3	5.8	0.35
P_2[d]	27.6	30.1	21.2	11.8	7.9	1.6			
$P°_2$	43.1	26.2	15.6	8.4	4.2	2.5			

[a] $\upsilon_{1,3} = \upsilon_1 + \upsilon_3$ and see section 2.2 for further details. [b] $P_{1,3}(0)$ is neglected. [c] $P_{1,3}(0)$ from linear surprisal plot. [d] Bending distribution in $\upsilon_{1,3} = 0$ is assumed to be similar to the one in $\upsilon_{1,3} = 1$ for $\upsilon_2 = 0-3$ and is assigned by analogy to the prior distribution for $\upsilon_2 = 4-6$. [e] Data were taken for two sets of conditions to isolate the primary reaction, see text.

to be described below, and $P_{1,3}(0) = 21.2 \pm 3.9$. The full distribution has its maximum population, about 50%, in $\upsilon_{1,3} = 1$. The bending distribution in $\upsilon_{1,3} = 0$ was estimated by assuming a similarity to the $\upsilon_{1,3} = 1$ distribution plus a geometric progression with a decrease by a factor of 0.5 for the energetically allowed (050) and (060) states. The global bending distribution decreases with υ_2, although the bending distribution for the $\upsilon_{1,3} = 1$ stretching state has a slight maximum in $\upsilon_2 = 1$. The H_2O distribution obtained from analysis of a spectrum obtained for $[H_2] > [NO_2]$ is shown in the bottom half of Table 2. Satisfactory agreement exists between the distributions obtained from the two sets of experimental conditions, and the distributions given in Table 2 can be taken as nascent vibrational populations of H_2O from reaction 1, except for the equilibration between the ν_1 and ν_3 levels.

To measure a full HOD spectrum, including the important $\Delta\nu_1 = -1$ plus $\Delta\nu_2 = -2$ emission in the 2400−3000 cm^{-1} region, an experiment with $[D_2] > [NO_2]$ was selected with $[NO_2] = 2.2 \times 10^{13}$ and $[D_2] = 4.3 \times 10^{13}$ molecules cm^{-3} for which the only important secondary reaction is (5). The $\Delta\nu_3 = -1$ and $\Delta\nu_2 = -2 + \Delta\nu_1 = -1$ spectrum recorded at 0.5 Torr, together with the spectrum calculated with the distribution given in the lower part of Table 3, is shown in Figure 5b and 5c. The $P_3(\upsilon_3{=}1-3)$ distribution, which measures the energy in the newly formed O−H bond, has nearly equal populations in the $\upsilon_3 = 1$ and 2 states. Simulation of the 2400−2800 cm^{-1} band allows $P_3(\upsilon_3{=}0)$ to be experimentally determined. Populations in the "dark" 000 and 010 states were assigned by analogy to the statistical distribution in $\nu_{1,2}$. The uncertainty of this assignment cannot exceed half of the population in the dark states, and the resulting $P_3(0)$ contribution is 24.9 ± 3.1. This value agrees with $P_{1,3}(0)$ assignment for H_2O, confirming the validity of the linear surprisal extrapolation (vide infra). An experiment with $[NO_2] \gg [H_2]$ also was analyzed, and the result is shown in the top half of Table 3. The agreement between the vibrational HOD distributions from the two different experimental conditions is satisfactory.

We conclude that the vibrational distributions for H_2O and HOD from reaction 1 are self-consistent. The strong inverse correlation between stretching and bending excitation of H_2O and HOD demonstrated in Tables 2 and 3 is characteristic of

TABLE 3: Vibrational Distribution of HOD from the Reactions of OD with CH_2O

	$v_{1,2}$[a]										
v_3	0	1	2	3	4	5	6	7	P_3	P_3[b]	P_3°
					$[NO_2] \gg [H_2]$[c]						
0	5.7	4.3	6.2	3.1	3.7	1.1	1.4	0.9	26.4	29.5	75.9
1	9.6	8.8	9.0	3.6	2.3	3.3	1.0		37.6	36.0	20.6
2	14.0	8.1	4.8	2.9	3.8				33.6	32.2	3.32
3	1.7	0.7							2.4	2.3	0.11
$P_{1,2}$	31.0	21.9	20.0	9.6	9.8	4.4	2.4	0.9			
$P°_{1,2}$	21.2	15.2	21.1	14.0	13.1	7.4	5.2	2.6			
					$[NO_2] \ll [H_2]$[c]						
0	6.1	4.3	6.7	3.1	1.5	1.2	1.4	0.2	24.9	27.7	75.9
1	11.4	8.0	7.4	4.0	2.9	2.2	1.9	1.1	36.3	34.9	20.6
2	15.5	8.1	4.8	3.3	4.1	0.9			36.6	35.2	3.32
3	1.7	0.6							2.3	2.2	0.11
$P_{1,2}$	34.7	21.0	18.9	10.4	8.5	4.3	3.3	1.3			
$P°_{1,2}$	21.2	15.2	21.1	14.0	13.1	7.4	5.2	2.6			

[a] See section 2.2 for definition of $v_{1,2}$. [b] $P_3(0)$ from linear surprisal plots. [c] Data were taken for two sets of conditions to isolate the primary reaction, see text.

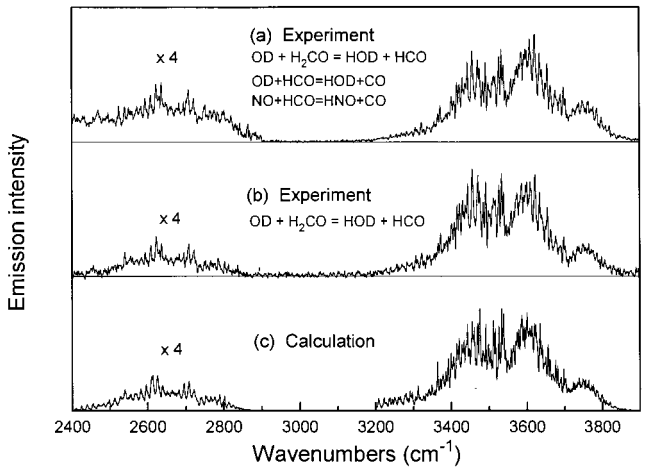

Figure 5. Spectra of HOD, adjusted for wavelength response, measured at 0.5 Torr ($\Delta t = 0.25$ ms): (a) $[NO_2] = 2.8 \times 10^{13}$ and $[D_2] = 1.8 \times 10^{13}$ molecules cm^{-3} (OD + H_2CO and OD + HCO reactions) and (b) $[NO_2] = 2.2 \times 10^{13}$ and $[D_2] = 4.3 \times 10^{13}$ molecules cm^{-3} (OD + H_2CO reaction). The calculated spectrum (c) corresponds to the vibrational distribution in Table 3.

the H_2O(HOD) distributions from H abstraction reactions by OH radicals.[14−17] The slightly more inverted P_3(HOD) distribution relative to the $P_{1,3}$(H_2O) distribution is commonly found;[15−17] the explanation is that the energy released to the old bond of H_2O is observed in the $P_{1,3}$(H_2O) distribution, but not in the P_3(HOD) distribution.

3.3. CO and CO_2 Distributions from the NO_2 + HCO Reaction. The response-corrected CO_2 spectrum from reaction 2 recorded at 0.5 Torr, $[NO_2] = 7.2 \times 10^{13}$ molecules cm^{-3}, and $[H_2] = 1.2 \times 10^{12}$ molecules cm^{-3} is shown in Figure 6a. The spectrum also has been corrected for a CO contribution to the lower wavenumber part of the spectrum by subtracting a model CO spectrum. The simulated spectra (Figure 6b) corresponds to $\Delta v_3 = -1$ emission from a ($v_{1,2}$) distribution. The average CO_2 "bending" distribution $P_{1,2}(v_2)$ obtained from fitting four experimental spectra is shown in the lower part of Figure 7a. All four spectra gave a distribution with a maximum population in $v_2 = 2$ with a declining tail that extended up to $v_2 = 13$. As previously noted, our simulation cannot identify the distribution in the ν_3 mode and levels above $v_3 = 1$ also could be excited.

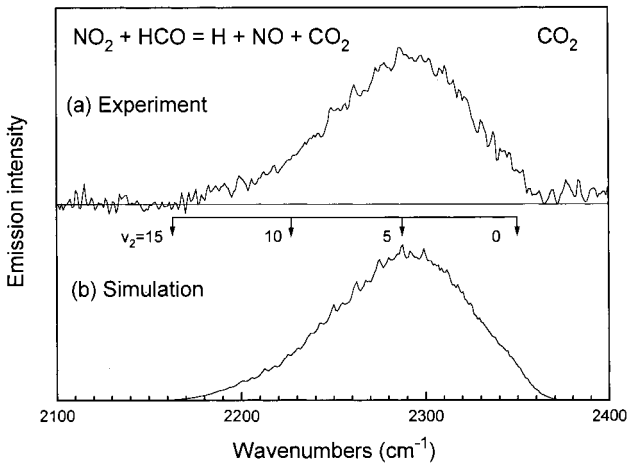

Figure 6. Simulation of a CO_2 spectrum from the NO_2 + HCO reaction: (a) observed spectrum at 0.5 Torr ($\Delta t = 0.25$ ms), $[NO_2] = 7.2 \times 10^{13}$, $[H_2] = 1.2 \times 10^{12}$ molecules cm^{-3}; (b) simulated spectrum corresponding to $v_3 = 1 \rightarrow 0$ transitions.

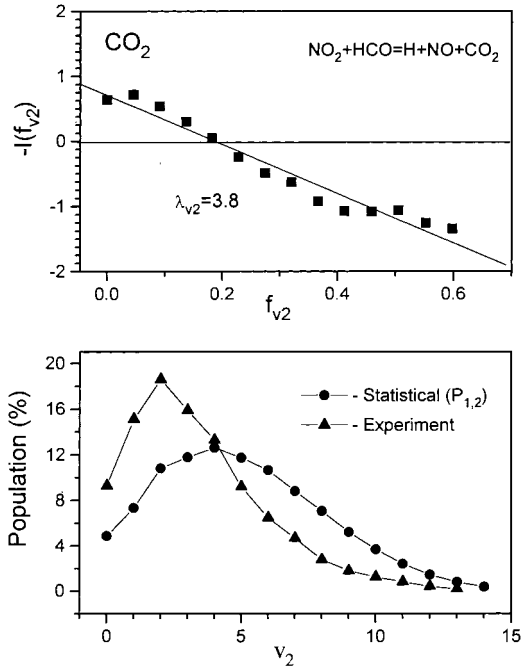

Figure 7. (a) CO_2($v_{1,2}$,v_3=1) distribution from the NO_2 + HCO reaction obtained by simulation (triangles) and the calculated statistical distribution (circles); (b) surprisal plot for the CO_2($v_{1,2}$,v_3=1) distribution from the NO_2 + HCO reaction.

The CO spectrum from reaction 2 recorded for the same conditions is displayed in Figure 8a. The best fit simulated spectrum is shown by the dotted curve and corresponds to a CO vibrational distribution of $P_v(1-4)$= 100:30:12:3. The least-squares parameter indicating the goodness of fit (Q) was quite small and this distribution is well established. The failure of a distribution composed of just $v = 1$ and 2 is displayed in Figure 8c. The $v = 0$ contribution can be estimated to be about 2.5 times larger that the $v = 1$ population from extrapolation of the distribution (or from a linear surprisal analysis).

No evidence for HNO emission was found in the spectra, and the range of vibrational excitation for CO_2 is more consistent with (2b) than the more exoergic (2c) channel. On the basis of the lack of observation of HNO emission and work by others, (2c) seems to have negligible importance. Observation of the 1−0 band of NO (Figure 3a) can be associated with either (2a′) or (2b). The formation of CO($v \geq 3$) requires that the other

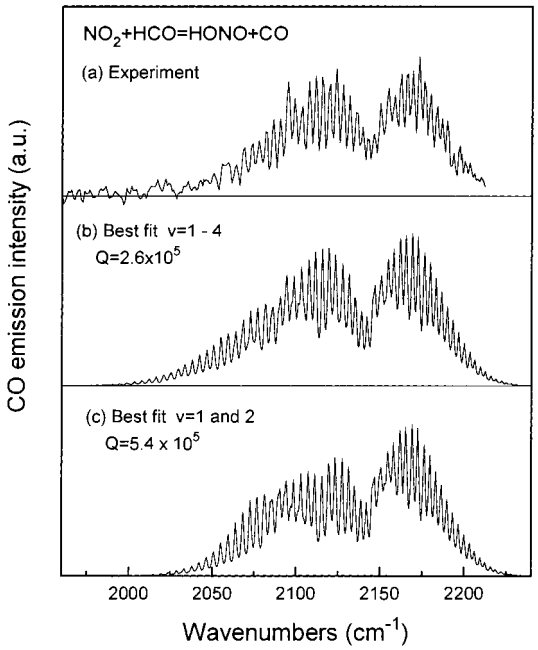

Figure 8. Comparison of experimental and simulated CO emission spectra from NO_2 + HCO reaction measured at 0.5 Torr. The simulated spectrum from using $v = 1$ and 2 clearly is not satisfactory. The best fit distribution is P(1−4) = 100:30:12:3.

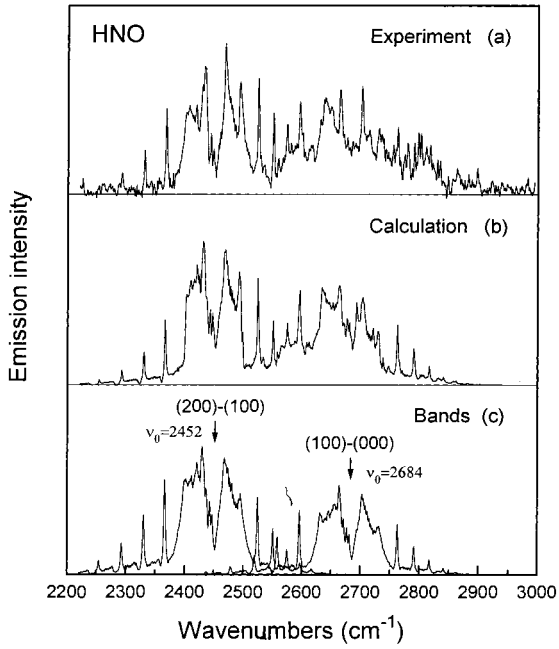

Figure 9. Comparison of experimental and simulated HNO spectra from the NO + HCO reaction: (a) experimental spectrum observed at 0.7 Torr with $[H_2] \approx [NO_2] = 3 \times 10^{13}$ molecules cm^{-3}; (b) fitted spectrum; (c) calculated ν_1 and $2\nu_1-\nu_1$ bands of HNO.

product in reaction 2 be HONO and not HO + NO. On the other hand, CO($v \leq 2$) molecules can be associated with either NO + OH or with HONO.

Knowing the $k_{2a} + k_{2a'}/k_{2b}$ ratio,[9,10] the experimental CO and CO_2 intensities can be used to estimate the fraction of CO_2 molecules in the $v_3 = 0$ state, $P_3(0)$. The average ratio of the CO to CO_2 integrated intensities obtained from four measured spectra was $I_{CO}/I_{CO_2} = 0.20 \pm 0.05$. The total concentrations are related as $[CO]/[CO_2] = (I_{CO}/I_{CO_2})(1 - P_3(0))(S_v(CO_2,\nu_3))/(0.5S_v(CO,1-0))$, where $S_v(CO,1-0) = 9.81 \times 10^{-18}$ and $S_v(CO_2,\nu_3) = 9.16 \times 10^{-17}$ cm^{-1}/(molecule cm^{-2}) are the absorption sum band intensities for the 1−0 band of CO and the ν_3 band of CO_2, respectively, which are known from the HITRAN database.[31] (A factor of 0.87 is needed to account for the small difference in CO and CO_2 band-center frequencies for emission intensities). The 0.5 factor in front of S_v(CO,1−0) reflects the CO vibrational distribution $P_v(0-5) = 64:25:8:3:1$ together with the vibrational Einstein coefficients 35.8, 68.8, 99.2, 127.0, and 175.2 s^{-1} for (1−0), (2−1), (3−2), (4−3), and (5−4) bands of CO, respectively.[26b] Assuming that $[CO]/[CO_2] = 1.5$, which agrees with the range of $k_{2a} + k_{2a'}/k_{2b}$ ratios from refs 9 and 10, we have $P_3(\neq 0) = 0.40 \pm 0.06$. Given the uncertainty associated with the $k_{2a} + k_{2a'}/k_{2b}$ ratio, our estimation is not very accurate; however, the data do suggest that a large fraction of the CO_2 molecules are in $v_3 = 0$.

3.4. HNO Distribution from the NO + HCO Reaction. When $[H] \approx [NO_2]$, the primary reaction is followed by the parallel reactions 3 and 4. Although both reactions give CO, we attribute the CO emission mainly to reaction 4 for two reasons. First, reaction 4 is an order of magnitude faster than reaction 3 and, second, the CO emission from reaction 2, which has a similar reaction rate, is rather weak (see Figure 1a). Consequently, only the HNO emission in the 2250−2900 cm^{-1} range was analyzed as a product from reaction 3.

The best conditions to obtain HNO emission from reaction 3 were $[H_2] \approx [NO_2] \approx 3 \times 10^{13}$ molecules cm^{-3} at 0.7 Torr, and a spectrum for such conditions is shown in Figure 9a. The bottom section, Figure 9c, shows the calculated (100)−(000) and (200)−(100) bands of HNO with equal populations in $v_1 = 1$ and $v_1 = 2$ states. The ν_1 fundamental of HNO corresponds to the H−N stretch mode. No emission from $v_1 = 3$ (band origin $\nu_0 = 2220$ cm^{-1}) was observed, though the available energy (∼35 kcal mol^{-1}) permits its excitation. Comparison of the calculated and measured hot $2\nu_1-\nu_1$ bands shows that emission from $v_1 = 2$ is not accompanied by bending excitation. However, the emission to the red of the ν_1 band origin can be attributed to the (110)−(010) and (101)−(001) bands. The ν_2(bend) and ν_3(NO stretch) levels are close in energy, 1501 and 1565 cm^{-1}, respectively, and they should be equilibrated by collisions with Ar for our conditions. The best visual fitting to the combination and hot bands was obtained with the following relative populations: (200):(100):(110):(101) = 100:60:50:35 (Figure 9b), assuming the Boltzmann ratio between the (110) and (101) states and that the Einstein coefficients for transitions from the $v_1 = 1$ and $v_1 = 2$ levels follow the harmonic oscillator approximation with a cubed frequency correction. The relative population of states with $v_1 = 1$ and 2 from fitting is about 14:10. The blue side of the spectra ($\nu >$ 2750 cm^{-1}) could be contaminated with emission from H_2CO excited in a V−V transfer processes between water and formaldehyde, and that emission was not interpreted.

The spectral shifts for two of the combination bands were obtained by matching several sharp peaks in the calculated and experimental spectra; the shifts were 69 cm^{-1} for the (110) and 27 cm^{-1} for the (101) vs the (100) band. These values, although rough, indicate that the HNO anharmonic coefficients are somewhat less than those ($x_{12} = -86.4$ and $x_{13} = -34.2$ cm^{-1}) obtained in ref 33.

3.5. The H_2O and CO Distributions from the OH + HCO Reaction. Both channels of reaction 4 are highly exothermic (see Table 1)

$$OH + HCO \rightarrow H_2O + CO \quad (4a)$$

$$\rightarrow H_2 + CO_2 \quad (4b)$$

and the absence of CO_2 emission indicates that channel 4b is

TABLE 4: Integrated Emission Intensities from H_2O and CO from Reactions 1 and 4 for Different Assumed Reaction Mechanisms for the Secondary Reaction (in Arbitrary Units)

experiment		abstraction[a]			elimination			
$I_{H_2O_{tot}}$	I_{CO}	$I_{H_2O_s}$	$I_{H_2O_p}$	$[H_2O_S]/[H_2O_P]$	$I_{H_2O_s}$	$I_{H_2O_p}$	$[H_2O_S]/[H_2O_P]$	$P_{1,3}$
103	30	52	51	1.0	32	71	0.73	*b*
					23	80	0.64	*c*
65	12	21	44	0.5	13	52	0.41	*b*
					9.4	56	0.38	*c*
$I_{HOD_{tot}}$	I_{CO}	I_{HOD_s}	I_{HOD_p}	$[HOD_S]/[HOD_P]$	I_{HOD_s}	I_{HOD_p}	$[HOD_S]/[HOD_P]$	P_3
232	27	143	89	1.6	67	165	0.86	*b*
					36	196	0.71	*c*
349	32	170	179	1.0	80	269	0.63	*b*
					38	311	0.54	*c*
249	30	158	91	1.7	74	175	0.90	*b*
					35	214	0.73	*c*

[a] Vibrational distributions of H_2O and HOD are the same as those from the primary reaction. [b] Vibrational distributions of H_2O and HOD are the same as those for unimolecular elimination of H_2O from ethanol. [c] Vibrational distributions of H_2O and HOD from reaction 4 determined from the difference spectra (see text).

not important. The CO spectrum from reaction 4 is very similar to the spectrum in Figure 2a and it is not shown. The CO(v) distribution declines with increasing v, $P(1-5) = 100:25:12:6:2$; the P_5 component has a large uncertainty, but emission from $v = 5$ does seem to be present. For this CO distribution, the surprisal analysis below gives $P(0) = 2.2P(1)$.

The water molecules produced in reaction 4 should give emission from which useful information about the reaction mechanism can be deduced. Since this water emission is overlapped by the emission from the primary reaction, the stoichiometric relation $[CO] = [H_2O]$ for reaction 4a was used with the spectra measured for conditions similar to the conditions of Figure 1c to separate the primary and secondary components giving water emission. This relation neglects the possible CO contribution from reaction 3; however, the ratio of rate constants of suggests that reaction 3 contributes only about 10%. The integrated intensity ratios from five independent experiments are $I[H_2O]_{tot}/I[CO] = 3.4$ and 5.3, and $I[HOD]_{tot}/I[CO] = 8.4$, 8.6, and 10.9 (see Table 4 for the data). The absorption band sum intensities are $S_v(1-0) = 9.8 \times 10^{-18}$ for CO, $S_v(\nu_3) = 7.2 \times 10^{-18}$ for H_2O, and $S_v(\nu_3) = 9.4 \times 10^{-18}$ cm^{-1}/(molecule cm^{-2}) for HOD,[23] which gives ratios of 1.0:2.2:2.9, respectively, for the fundamental emission band intensities (with adjustment by the cubed band-center frequencies). Next, the vibrational distributions must be taken into account, since equal concentrations can give different emission intensities depending on their vibrational distributions. The Einstein coefficients of CO($\Delta v = -1$) are 35.8, 68.8, 99.2, 127.0, and 175.2 s^{-1}, for transitions from $v = 1-5$, respectively.[26b] For $P_v(0-5) = 61:27:7:3.2:1.6:0.4$, the CO emission intensity is equal to 0.6 of $S_v(1-0)$. For estimation of the water emission intensity, some a priori distribution must be assumed. Two extreme cases were considered. First, the P_3 and $P_{1,3}$ stretching distributions were taken as those from reaction 1 (abstraction-like distribution), and the emission intensities from these distributions are $0.45S_v(\nu_3)$ for H_2O and $1.05S_v(\nu_3)$ for HOD. The second type, elimination-like distribution, were taken as those from ethanol decomposition,[35] $P_3(0-3) = 60:32:7:2$ and $P_{1,3}(0-3) = 50:33:14:4$; the emission intensities from these distributions are $0.28S_v(\nu_3)$ for H_2O and $0.49S_v(\nu_3)$ for HOD. Since most molecules are in υ_3 or $\upsilon_{1,3} = 0$ from an elimination reaction, the emission intensity is significantly less for an elimination-like distribution than for an abstraction-like distribution. Equal concentrations of CO, H_2O, and HOD would produce experimental intensity ratios of $I_{CO}:I_{H_2O}:I_{HOD} = 1.0:1.7:5.3$ for the abstraction case and 1.0:1.1:2.5 for the elimination case. The measured intensities for two H_2O spectra and for three HOD spectra together with calculated contributions to the water spectra from the primary, I_P, and secondary, I_S, reactions from an abstraction mechanism and from an addition−elimination mechanism for reaction 4 are given in Table 4. The $I_{H_2O,S}$ and $I_{HOD,S}$ are obtained by simple scaling of the I_{CO} values by the ratios above, and then the $I_{H_2O,P}$ and $I_{HOD,P}$ are obtained by the difference between I_{tot} and I_S. Since the abstraction-like distribution from (4) was assumed to be the same as from (1), the $I_{H_2O,S}$ and $I_{H_2O,P}$ ratio is the concentration ratio. However, for the elimination-like case the I_P and I_S must be adjusted for different distributions to obtain the concentration ratios in Table 4. Water production from the secondary reaction cannot exceed that of the primary product. However, three of the five experiments give $[H_2O]_S > [H_2O]_P$ for an abstraction mechanism. Thus, on the basis of just on the comparison of I_{CO} to I_{H_2O} and I_{HOD}, the abstraction mechanism seems to be ruled out. Numerical integration of the rate equations for the complete model, including reactions 1−4 for starting conditions of $[CH_2O] = (5-8) \times 10^{13}$, $[H_2] = (2-3) \times 10^{13}$, and $[NO_2] = 5 \times 10^{13}$ molecules cm^{-3} gives $[H_2O]_S/[H_2O]_P = 0.4$, which lends support to the $[H_2O]_S/[H_2O]_P$ values obtained from an elimination-like distribution.

Estimates for the vibrational distributions of H_2O and HOD from reaction 4 can be obtained by simulation of a spectrum obtained as a difference between the total H_2O(HOD) spectrum and the H_2O(HOD) spectrum from just the primary reaction. The latter were obtained by multiplying the H_2O and HOD spectra from the section 3.2 by a factor that gives an integrated intensity that matched the measured CO emission intensity. The derived distributions are $P_{1,3}(0-3) = 63:24:11:2$ and $P_3(0-3) = 76:20:4:0$, and $I_{CO}:I_{H_2O}:I_{HOD} = 1.0:0.8:1.3$. The populations in the $\upsilon_{1,3} = 0$ and $\upsilon_3 = 0$ states were estimated by extrapolation and from surprisal analysis. These distributions are just estimates, but they support an addition−elimination mechanism. Perhaps the most convincing argument is the comparison of the H_2O and HOD spectra from the primary reaction (Figures 4b and 5b) to the combined water spectrum from reactions 1 plus (4); see Figures 4a and 5a. Even when intense CO emission is observed from reaction 4, the combined H_2O and HOD spectra show no emission from $\upsilon_{1,3}$ or $\upsilon_3 \geq 4$. This strongly weighs against an abstraction mechanism, which should give H_2O(HOD) molecules with very high vibrational excitation.

3.6. The CO(v) Distribution from the H + HCO Reaction. This reaction is also highly exothermic and excitation of up to 14 vibrational quanta in the CO molecule is possible. Nevertheless, the highest observed state was $v = 5$ (Figure 2c). The simulated spectrum shown in Figure 2b corresponds to $P(1-5) = 100:25:11:5:1.5$, which is very similar to the CO distribution from reaction 4a. The reliability of this CO(v) distribution was discussed when the spectral simulation method for CO emission was presented.

4. Discussion

4.1. Surprisal Analysis and Energy Disposal for Reaction 1. Theoretic-information analysis[36,14] of the H_2O and HOD vibrational distributions from reactions 1 and 1D were done using the prior distributions, $P°_{1,3}$ and $P°_3$, for three models: (I) the radical fragment R (CHO) is treated as an atom; (II) the rotational degrees of freedom of R are taken into account; (III)

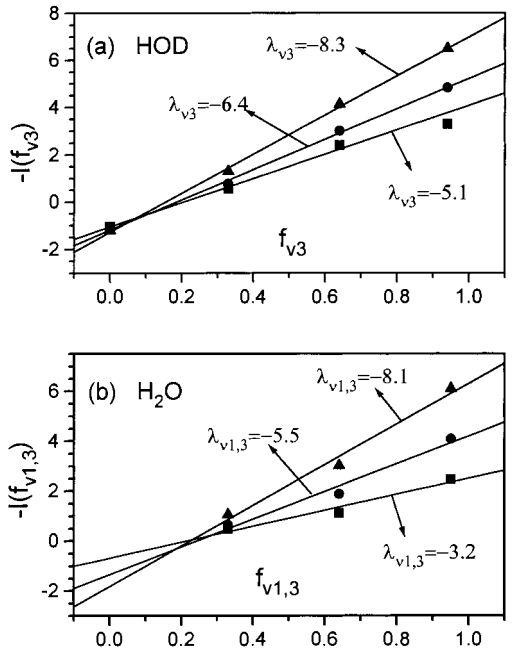

Figure 10. Surprisal plots for the stretching distributions of HOD (a) and H_2O (b) from the OH + CH_2O reaction. The three models for the priors are given in the text.

rotational and vibrational degrees of freedom of R are included in calculation. The surprisal plots for HOD(a) and H_2O(b) for all three models are shown in Figure 10, and Tables 2 and 3 contain prior distributions for model I. The average experimental distributions, $P_{1,3}$ and P_3, from simulation of four H_2O and four HOD independent spectra were used to make the surprisal plots.

The HOD surprisals, which are plots of $-\ln(P_3/P^\circ_3)$ vs $f_{v3} = E_{v3}/\langle E_{av}\rangle$, summarize the deviation of the excitation in the newly formed H−OD bond from the statistical expectation. The surprisal plots for OD + CH_2O are linear, and $-\lambda_{v3} = 5.1 \pm 0.4$ with an intercept of $\lambda^\circ_3 = -0.97 \pm 0.12$ for model I prior, giving a renormalized distribution $P_3(0-3) = 29{:}36{:}32{:}2$ in agreement with the experimental average value of $P_3(0) = 26 \pm 4$. The H_2O surprisal plot also is linear, and the slope from model I prior is $-\lambda_{v1,3} = 3.2 \pm 0.4$, which is less than for HOD because the ν_1 and ν_3 normal mode populations include the "active" and "spectator" local O−H mode vibrations. The intercept, $\lambda^\circ_{1,3} = -0.67 \pm 0.23$, gives a renormalized distribution of $P_{1,3}(0-3) = (21 \pm 4){:}50{:}28{:}5$.

Surprisal plots using model II and III priors (Figure 10) also are linear but with steeper slopes than for model I and $-\lambda_{v3}$ equals 6.4 ± 0.2 and 8.3 ± 0.2, and $-\lambda_{v1,3} = 5.5 \pm 0.9$ and 8.1 ± 1.0 for models II and III, respectively. The $P_3(0)$ and $P_{1,3}(0)$ populations derived from the intercepts of the models II and III plots are lower than that for model I. On average, these estimates show less agreement with the measured population of HOD than the model I extrapolation, and that is why the $P_{1,3}(0)$ values for H_2O were estimated using the model I prior. Nevertheless, the acquisition of some rotational and vibrational energy by HCO cannot be ruled out, and the actual $P_3(0)$ and $P_{1,3}(0)$ values may be intermediate between the predictions of models I and II.

In order to assign the global bending distributions for H_2O, the ν_2 distribution in $v_{1,3} = 0$ was assumed to be similar to that for $v_2 = 0-3$ of $v_{1,3} = 1$ and the $v_3 \geq 4$ populations were assigned by analogy to the prior distribution (note that $v_2 = 6$ is included with $v_2 = 5$ in Table 2). Having the total vibrational distribution, the fraction of the energy released as vibrational energy was found to be $\langle f_v(H_2O)\rangle = 0.56 \pm 0.03$, with the component in bending $\langle E_{2v}\rangle/\langle E_v\rangle = 0.34$, and $\langle f_v(HOD)\rangle = 0.54 \pm 0.02$, with the component released to the O−H stretch vibration $\langle E_{3v}\rangle/\langle E_v\rangle = 0.63$. The experimental bending distribution is just slightly more inverted than the prior distribution; see Table 2. The energy disposal data from reaction 1, along with the results for several other related hydroxyl radical reactions, are summarized in Table 5. Since model II surprisal plots give slightly smaller λ°, a slightly higher $\langle f_v\rangle$, closer to 0.6, could be selected for CH_2O.

The energy disposal pattern for CH_2O closely resembles those from H_2S and HBr, which also have very similar available energies. The 300 K rate constants (per H atom) decline in the series HBr (11×10^{-12} cm^3 s^{-1}), H_2CO (4.8×10^{-12} cm^3 s^{-1}), and H_2S (2.4×10^{-12} cm^3 s^{-1}). The ratio of stretch-to-bend excitation for HBr and H_2CO are the same (∼2), and that for H_2S is somewhat higher (3.1). The energy disposal pattern of the OH + CH_2O reaction also closely resembles that from $(CH_3)_2S$, even though the available energy is 6 kcal mol^{-1} larger and the rate constant (per C−H bond) is 6 times larger for CH_2O. The reaction of OH with representative hydrocarbons demonstrate a somewhat higher overall $\langle f_v(H_2O)\rangle$ with a much larger stretch-to-bend excitation ratio (∼5). The slopes of the surprisal plots (model I prior) of CH_2O, or $(CH_3)_2S$, are lower than that from C_4H_{10} or cyclo-C_6H_{12} reactions because the distributions from the hydrocarbons are much more inverted.

TABLE 5: Summary of Energy Disposal for OH, OD, and F + HR Reactions

reaction	$\langle E_{av}\rangle$[a]	$-\lambda_{vn}$[b] I	II	III	$\langle f_v\rangle$	$\langle E_{vs}\rangle$[c]/$\langle E_v\rangle$	ref
OH + CH_2O → H_2O + HCO	33.2	3.2	5.5	8.1	0.56	0.34	
OD + CH_2O → HOD + HCO	33.5	5.1	6.4	8.9	0.54	0.63	
OH + DMS → H_2O + CH_3SCH_2	27.5	3.2	5.3	8.9	0.53	0.30	17
OD + DMS → HOD + CH_3SCH_2	27.8	4.9	6.3	9.2	0.55	0.64	
OH + HBr → H_2O + Br	33.7	4.5			0.61	0.30	14
OD + HBr → HOD + Br	34.0	6.1			0.63	0.61	
OH + C_6H_{12} → H_2O + C_6H_{11}	27.1	5.7	8.2		0.62	0.14	16
OH + C_4H_{10} → H_2O + C_4H_9	24.7	5.5	8.4	9.8	0.65	0.19	
OD + C_6H_{12} → HOD + C_6H_{11}	27.4	6.3	8.6		0.56	0.82	
OD + C_4H_{10} → HOD + C_4H_9	25.0	6.3	8.6	10.4	0.59	0.79	
F + CH_2O → HF + HCO	52.0	4.4	8.0		0.56		56
		4.6[d]	8.8[d]		0.59		57

[a] In kcal mol^{-1}. Available energies for deutero-isotopic reactions were calculated accounting for a change in zero vibration energies. [b] Model I neglects the internal degrees of freedom of the product radical in the calculation of prior distribution; model II includes rotations of the radical fragment and model III includes three vibrational modes to facilitate comparison to OH + H_2CO. [c] The fraction of the total vibrational H_2O energy released to bending mode, $\langle E_{v_2}\rangle/\langle E_v\rangle$, in reactions with OH and the fraction of HOD vibrational energy found in O−H mode, $\langle E_{v_3}\rangle/\langle E_v\rangle$, for reactions with OD. [d] Calculated from the data in Figure 5 of ref 57.

A "pure" model III prior is not a convenient reference because of the different number of vibrational modes in the R fragments, and calculations were made for a reduced number of degrees in order to compare the surprisals. The $-\lambda_v$ values for model III in Table 5 correspond to 3 vibrations in R═CH_3SCH_2 (C−H stretching, C−S stretching, and CH_2 group bending) and R═C_4H_9 (C−H stretching, C−C stretching, and CH_2 group bending). The $-\lambda_v$ values for the C_4H_{10} reaction are somewhat larger than for CH_2O or $(CH_3)_2S$ for all three priors. From all points of view, the $\langle f_v \rangle$ and λ_v values indicate that reaction 1 proceeds via direct abstraction of an H atom, but with more bending excitation in the H_2O product than from reactions with secondary C−H bonds of hydrocarbons (the same statement applies to primary C−H bonds, but the number of examples is small).

The question of whether HCO from reaction 1 contains enough vibrational energy to enable decomposition to H + CO has been asked.[16] We did observe the characteristic $K = 2,3,4$ ^qQ-peak of the C−O vibrational mode of HCO at 1867 cm^{-1} [34] (see Figure 3b). For these conditions the steady-state HCO concentration is about 0.8 of the concentration of the primary H_2O product. The ratio of the integrated emission intensities of HCO(ν_3) and HOD(ν_3) is roughly 1/50. Assuming approximately equal sum intensities for these bands, the estimated yield of HCO(υ_3=1) is an order of magnitude less than HOD(ν_3). The CH stretching fundamental (ν_1) of HCO with band origin at $\nu_0 = 2434.5$ cm^{-1} [37] was not detected in our experiments. Its detection is complicated by the overlapping with HNO $2\nu_1-\nu_1$ hot band ($\nu_0 = 2452$ cm^{-1}), but the strongest peak of $K = 3$ ^qQ-branch at 2419.1 cm^{-1} [37] was not observed under any conditions. The peak absorptions of equivalent a-type transitions in ν_1 and ν_3 of HCO have virtually the same strength.[34] Thus, we can conclude that HCO(υ_1=1) was not present. Even the CO stretch emission was extremely weak and the degree of vibrational excitation of HCO certainly is minor. The equilibrium geometries of CH_2O and HCO are similar,[25a] ∠HCO = 122° and 123°, R(C−O) = 1.20 and 1.18 Å, and R(C−H) = 1.12 and 1.15 Å, respectively, and the amount of radical stabilization energy is not expected to be large. As for most direct H-atom abstraction reactions,[18b] the energy released as internal energy of the R group is small and most of the available energy is divided between the newly formed bond (including bending) and relative translational energy.

According to ab initio calculations at the MCHF/CI[38] and PMP4/SDTQ/311G**[39] levels of theory, the barrier for H abstraction in (1) is 1.2 kcal mol^{-1}. The transition state (TS) geometry corresponds to R(O−H) = 0.967 Å, R(O−H′) = 1.395 Å (+43.8%), R(C−H′) = 1.180 Å (+6.7%), ∠O−H′−C = 168.4°, and ∠H−O−H′ = 94.5° (−9.6%).[39] The figures in parentheses show the deviation from the equilibrium parameters of H_2O or CH_2O. The structure of the TS is reactant-like in character and shows a strong H′ vector in the direction of the O atom, which is consistent with release of 35% of the available energy to stretching excitation of the newly formed O−H′ bond. The transition states for H-atom abstraction from H_2CO, $(CH_3)_2S$,[40] ethane,[41] and propane[42] are similar and correspond to nearly collinear H′ atom geometry (∠O−H′−C = 166.2° for $(CH_3)_2S$ and 176.7° for the secondary H′ abstraction of propane) with the H−O−H′ angle (94.8° in $(CH_3)_2S$ and 95.6° in propane) rather close to the equilibrium angle of H_2O (104.5°). The geometry of these transition states does not provide any clues about why the stretch-to-bend excitation of H_2O depends on reactant. Actually, the entrance channel potential for H_2S and H_2CO probably resembles that of HBr more than those of the hydrocarbons, because these three reactants have nearly zero activation energy. In addition to effects arising from the differences in entrance channels and available energy, the higher bending excitation from CH_2O, HBr, H_2S, and $(CH_3)_2S$, compared to hydrocarbons, could be the result of interaction between the polar H atoms of water with the lone electron pairs of the O (or S, or Br) atom of the product fragment in the exit channel; i.e., exit channel dynamics associated with attractive interactions may steal energy from the stretch mode.[43]

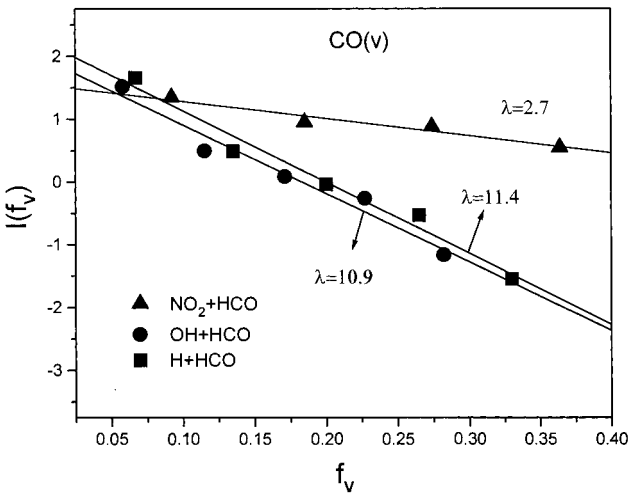

Figure 11. Surprisal plots for CO from OH + HCO (circles), H + HCO (squares), and NO_2 + HCO (triangles) reactions.

4.2. Reaction of OH with HCO. Gutman and co-workers[8] suggested that the OH + HCO reaction might proceed by association of OH with HCO followed by decomposition of formic acid. However, the activation energy for abstraction of the weakly bound H atom must be negligible, given the rate constant for OH + H_2CO, and the question of whether reaction 4a proceeds solely by association without a contribution from direct abstraction at room temperature must be addressed.

$$\mathrm{OH + HCO \rightarrow HC(O)OH \rightarrow H_2O + CO} \qquad (4a)$$

$$\mathrm{\rightarrow H_2 + CO_2} \qquad (4b)$$

The infrared multiphoton dissociation of formic acid has been studied[44] by excitation of both the C−H and C═O stretch modes, 98% of the reaction proceeded by (4a). According to two independent ab initio studies[45,46] the activation energy is lower for dehydration (63.0 and 68 kcal mol^{-1}) than for decarboxylation (65.2 and 71 kcal mol^{-1}). On the basis of the absence of CO_2 emission for conditions optimizing reaction 4, plus the information above, we dismiss (4b).

The direct abstraction process would be expected to give $\langle E_v(H_2O) \rangle \approx 50$ kcal mol^{-1} with vibrational excitation extending to 70−90 kcal mol^{-1}. Although the H_2O and HOD distributions from (4a) were not measured with high reliability, the emission did not extend to $\upsilon = 4$ (Figures 4c and 5c) and the distributions are totally inconsistent with a direct abstraction reaction. The estimated experimental $\langle E_v(H_2O) \rangle \approx 11$ kcal/mol ($\langle f_v \rangle$ is 0.1) and the vibrational distributions are as expected for unimolecular elimination of water using ethanol ($\langle f_v(H_2O) \rangle = 0.15$) and acetic acid ($\langle f_v(H_2O) \rangle = 0.24$) reactions as examples. The vibrational distribution for CO from (4a) also can be examined. A linear surprisal plot was used to estimate $P(0)$ (see Figure 11), giving $P(0-5) = (60.8 \pm 4.5)$:27.1:6.9:32:1.6:0.4. The average vibrational energy is 3.6 kcal mol^{-1} and $\langle f_v \rangle = 0.036$; the excitation is very modest, and even below the statistical value,

TABLE 6: Vibrational Distributions of CO from the Reactions of HCO[a]

reaction	$v = 0$[b]	$v = 1$	$v = 2$	$v = 3$	$v = 4$	$v = 5$	$v = 6$	$\langle E_v \rangle$	$\langle f_v \rangle$	λ_v[b]	ΔS
NO_2 + HCO	64.0	24.7	7.5	2.9	0.8			3.1	0.047	2.7	0.07
$P°(v)$	54.5	26.0	11.7	4.9	1.9	0.6					
OH + HCO	60.8	27.1	6.9	3.2	1.6	0.4		3.6	0.036	10.9	0.70
$P°(v)$	30.4	21.8	15.5	10.8	7.5	5.1					
H + HCO	62.1	27.1	5.8	3.0	1.5	0.4		3.4	0.037	11.4	1.12
$P°(v)$	23.7	19.0	15.0	11.7	9.0	6.8					
F + HCO	48.3[c]	27.4	12.4	6.2	3.8	1.8		5.8	0.049	9.0	0.98
	37.4[d]	35.7	10.6	6.3	3.9	2.9	1.8	7.5	0.064	6.4	0.76
$P°(v)$	19.1	16.0	13.4	11.0	9.1	7.4	5.9				

[a] $\langle E_v \rangle$ in kcal mol^{-1}; the available energies are 66.7, 106.5, and 91.1 kcal mol^{-1} for the NO_2, OH, and H reactions, respectively; ΔS in cal mol^{-1} K^{-1}. [b] $P_v(0)$ was obtained from linear surprisal plots using the full priors for each reaction, including all modes of HONO for reaction 2. [c] Reference 58. [d] Our unpublished data.

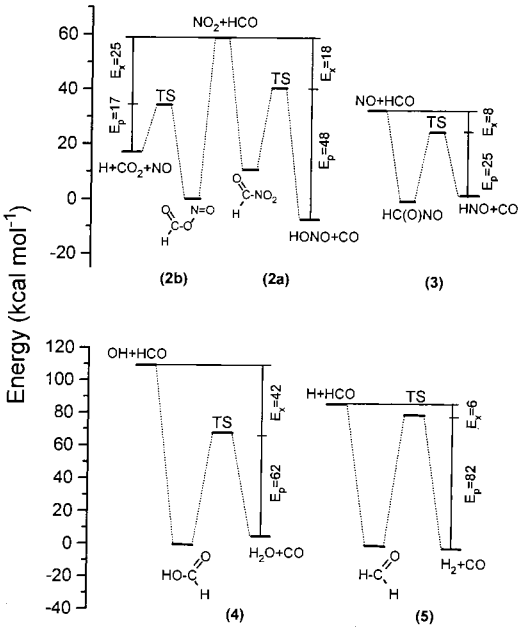

Figure 12. Energy diagram for CO forming reactions of formyl radical: NO_2 + HCO (2a) (ref 9); NO + HCO (3) (ref 11); OH + HCO (4) (ref 46); and H + HCO (5) (ref 49). The potential energy given for CO_2 formation (2b) from HCO + NO_2 is the sum for the two consecutive dissociation processes; the majority (13 kcal/mol) is associated with the decomposition of HCO_2 (see text of the Discussion section).

$\lambda_v = 10.9$ (see Table 6). The sum rule[47] states that the vibrational energy available to H_2O and CO may be expressed as $\langle E_v \rangle = aE_x + bE_p$. For a RRKM process, E_x is distributed statistically among the TS vibrational modes, implying $a = 0.33$ for H_2O and $a = 0.11$ for CO. As shown in Figure 12(4), the unimolecular process releases 42 kcal mol^{-1} as E_x and 62 kcal mol^{-1} as E_p. Evidently the unimolecular decomposition of formic acid mainly converts E_p to relative product translational energy. Just as for hydrogen halide elimination, three-centered elimination processes seem to convert less E_p to vibrational energy of H_2O than do four-centered elimination reactions.

The rate constant for H abstraction from HCO by OH surely is equal to or greater than that for H_2CO (per H atom) and an upper limit should be the value for HBr (1.1×10^{-11} cm^3 s^{-1}). The OH + HCO reaction rate constant is $>5 \times 10^{-11}$ cm^3 s^{-1},[2,3] which implies that the association channel is dominant. Both processes should have zero activation energy, and the difference in rate constants must be associated with the requirement for the p-orbital of the OH′ radical to be aligned with the H−C bond with a rather specific angle between the OH′ and the H−C−O axis for successful abstraction. The reduction in reaction cross section for rotational excitation of either OH or HBr should be noted in this context.[43] The steric requirements are apparently much less severe for the radical−radical addition process.

4.3. Reaction of H with HCO. Reaction 5 has been discussed in terms of association of H with HCO, with subsequent unimolecular decomposition of formaldehyde, and direct abstraction:

$$\mathrm{H + HCO \rightarrow H_2CO \rightarrow H_2 + CO}$$
$$\mathrm{\rightarrow H_2 + CO} \qquad (5)$$

According to Harding and Wagner's variation transition-state calculations on a reliable global potential surface,[48] the addition channel dominates over abstraction by a factor of 5 at room temperature, just as we discussed for OH + HCO. However, the competition between redissociation of H_2CO and elimination of H_2 must be evaluated. Harding and Wagner used RRKM theory with threshold energies of 87.0 and 83.5 kcal mol^{-1} for dissociation and elimination (respectively) and found that the elimination channel became slightly (45%) less important than abstraction (55%). However, the current assignments of the threshold energies are 87.3 and 79.2;[49] the reduced threshold energy for elimination would make recombination−elimination the more important pathway by a factor of 2, according to the results of Figure 8 of ref 48. We will discuss our data as if the reaction was recombination−elimination, but a 10−25% contribution from direct abstraction may exist.

The prior distribution for CO from reaction 5 calculated by integration over the rotational states of H_2 and CO is given in Table 6. The surprisal plots for CO from reactions 5 and 4 in Figure 11 are nearly identical. The intercept was used to obtain P(0), and the distribution is $P(0-5) = (62.2 \pm 5.0)$:27.1:5.8:3.0:1.5:0.4 with $\lambda_v = 11.4$. The vibrational energy is 3.4 kcal mol^{-1} and $\langle f_v \rangle = 0.037$. The energy released to CO is very similar for reactions 4 and 5.

The unimolecular decomposition of formaldehyde has been studied in great detail following photoexcitation.[49−53] Since internal conversion follows excitation to S_1, our chemical activation results can be compared to the photoexcitation experiments for $\lambda \approx 314$ nm. The CO distributions have been determined by vacuum UV laser-induced fluorescence following photoexcitation at 339 nm.[50] The $P(1)$:$P(0)$ ratio was 0.17 and no signals were seen for CO($v>1$). The rotational distribution was highly nonthermal with $25 < J < 63$ and a maximum population at $J = 42$ for both $v = 0$ and 1. In earlier work Cheng et al.[51] showed that the vibrational distribution depended on the photolysis wavelength and at 317 nm (90 kcal mol^{-1}) the P_0-P_2 values were 77:19:4, which resembles our results. The classical trajectory study of the dissociation of H_2CO using a potential surface calculated by the empirical valence-bond

method[54] gave product state distributions that matched the experimental results. Similar vibrational, $P(0{:}1) = 82{:}18$, and rotational, $J_{max} = 50$, distributions for CO were also obtained in a combined ab initio plus classical trajectory calculations for the unimolecular decomposition of H_2CO,[55] although the potential energy barrier height was ~25 kcal mol^{-1} larger than the experimental result.

Let us compare energetics for reactions 4 and 5, assuming that they proceed via the recombination−elimination mechanism (Figure 12). One difference is the 23 kcal mol^{-1} higher energy for HCOOH because D(H−CHO) = 87 kcal mol^{-1} and D(HO−CHO) = 110 kcal mol^{-1}. As a result, formic acid has $E_x = 42$ kcal mol^{-1}, while formaldehyde has only about 8 kcal mol^{-1} of excess energy. From the analysis of reaction 4, the vibrational excitation of CO was attributed to the statistical redistribution of E_x. The statistical component is about 4.6 kcal mol^{-1} for H_2O + CO, but only 1.3 kcal mol^{-1} for H_2 + CO. Since the $\langle E_v(CO)\rangle$ are nearly the same, the H_2CO reaction converts some of the E_p to CO vibrational energy, as well as to rotational energy ($\langle E_R(CO)\rangle \approx 10$ kcal mol^{-1}). The strong rotational excitation from H_2CO decomposition is a consequence of the impulsive interaction of H_2 with the carbon end of CO.[50,54]

The results from reactions 4 and 5 also can be compared with the CO vibrational distribution from the F + HCO → HF + CO reaction,[58] which also proceeds by an addition−elimination mechanism with $\lambda_v = 9.0$ and $\langle f_v\rangle = 0.049$ as calculated from the P(v) of Donaldson and Sloan. These results closely resemble the energy disposal for reactions 4 and 5. The calculated entropy deficiency values are also rather close for all three reactions, ΔS(cal mol^{-1} K^{-1}) = 0.70 for reaction 4, 1.12 for reaction 5, and 0.98 for F + HCO.

4.4. Reactions of NO_2 and NO with HCO. *NO_2 + HCO*. The mechanism for reaction 2 is thought to be recombination with formation of either N(O)C−NO_2 or H(O)C−ONO[9,10] (Figure 12).

$$NO_2 + HCO \rightarrow H(O)C{-}NO_2 \rightarrow HONO + CO \quad (2a)$$

$$\rightarrow HO + NO + CO \quad (2a')$$

$$\rightarrow H(O)C{-}ONO \rightarrow H + CO_2 + NO \quad (2b)$$

reaction has been studied by Guo et al.[9] by laser flash-kinetic spectroscopy and modeled with RRKM theory using frequencies and threshold energies from ab initio calculations. The CO_2 product was measured, and its yield was determined to be 52 ± 14%; the HONO product was detected, and some vibrationally excited CO_2 was also observed by monitoring the R(16) line in the (111)−(010) band. Rim and Hershberger[10] have used infrared diode-laser spectroscopy to measure CO, CO_2, and NO from reaction 2, and they conclude that (2a′) accounts for 63 ± 5%, (2b) for 37 ± 5%, and (2a) or (2c) for less than 10% around 1 Torr pressure. Our data give a CO(v=0−4):CO_2(P_3(1)) concentration ratio of 4:1. With $CO_2(P_3(0)) \approx 60\%$ the ratio would decline to 4:2.5, and our data are in accord with the upper limit for (2a + 2a′):(2b) branching ratio of Guo et al. and with the lower limit of Rim and Hershberger. The above estimation of $P_3(0)$ is consistent with the CO_2 statistical distribution $P^\circ_3(0-4) = 71.9{:}21.8{:}5.3{:}0.9{:}0.1$; six translational and four rotational degrees of freedom with direct summation of states for NO and CO_2 vibrations were used for the prior of (2b). Our only reservation is the importance of (2a) vs (2a′). Since formation of CO($v \geq 3$) can occur only for (2a), the observed CO vibrational distribution proves that the HONO + CO channel has some importance. Channel 2a′ represents HONO molecules that were formed above the dissociation limit, which is open for CO($v \leq 2$). In order to obtain an idea about the possible fraction of CO molecules with $v = 0-2$ from (2a), we examined the statistical distribution with $E_{av} = 66.7$. The prior (Table 6) was calculated by direct summation over the vibrational levels of HONO (with the vibrational frequencies of the trans isomer) and rotation levels of CO and integration over the HONO rotational energy. The surprisal plot presented in Figure 11 is linear; the intercept, $\lambda_0 = 1.56 \pm 0.12$, allows estimation of the $P_v(0)$ component and the full CO vibrational distribution is $P_v(0-3) = (64 \pm 3){:}25{:}8{:}3{:}1$ (Table 6). The slope of the surprisal plot, $\lambda_v = 2.7 \pm 0.4$, is small and positive, indicating that the experimental CO distribution is slightly colder than the statistical distribution. Since CO retains less than the statistical fraction of energy, a large fraction of the HONO molecules could retain enough energy for subsequent decomposition, providing that the rearrangement step is not repulsive in nature; i.e., negligible translational energy is released to the products. Additional experimental or theoretical characterization of the H(O)C−NO_2 rearrangement is needed to confirm Rim and Hershberger's claim that (2a′) is more important than (2a).

The decomposition of H(O)C−ONO proceeds stepwise by rupture of the O−N bond followed by the decomposition of H−CO_2.[59] The last step has a net change in potential energy of 13 kcal mol^{-1},[59] which is mainly associated with the change in geometry as the CO_2 bending coordinate relaxes to 180°. In spite of the small potential energy release, CO_2 still acquires considerable bending vibrational energy in the sum of the two steps. Since the observed CO_2 distribution corresponds to $2\nu_2-\nu_1$ mode equilibration in $\nu_3 = 1$, the prior also was calculated for complete $2\nu_2-\nu_1$ equilibration. The $P^\circ_{1,2}$ prior distribution and the surprisal are shown in Figure 7; the surprisal is approximately linear with $\lambda_{v2} = 3.8$, which means that the bending excitation is less than statistical. Assuming that all molecules are in $\nu_3 = 1$ state, the experimental $P_{1,2}$ distribution gives $E_v(CO_2) = 13.0$ kcal mol^{-1} and $\langle f_v\rangle = 0.31$, which are essentially the same as the statistical values, $E_vo(CO_2)$=13.8 kcal mol^{-1} and $\langle f_v^0\rangle = 0.33$, as might be expected for two consecutive dissociative processes.

NO + HCO. Reaction 3 proceeds through the HC(O)NO intermediate with formation of HNO by unimolecular rearrangement rather than by a direct hydrogen abstraction.[11] Since this reaction is thermoneutral, E_0 is equal to E_P (see Figure 12). The complete absence of the energetically allowed $\nu_1 = 3$ (22.3 kcal mol^{-1}) or $\nu_1 = 1$, $\nu_2 = 2$ (16.4 kcal mol^{-1}) states serves as confirmation of the unimolecular mechanism, since direct abstraction reactions tend to give vibrational energy in the new bond that extends to the thermochemical limit. Comparing the measured ratio of HNO populations in $\nu_1 = 1$ and 2 with the total statistical population in the ν_1 mode, $P_1(0-3) = 65{:}24{:}8{:}2$ and, assuming a linear dependence of the surprisal upon $\langle f_v\rangle$, a noninverted N−H stretch distribution, $P_1(0-3) = 40{:}35{:}25{:}0$, can be estimated. The energy released to HNO was estimated with the assumption that the $\nu_2 = 0$, 1, and 2 bending states of $\nu_1 = 0$ are equally populated. Thus, $\langle E_v\rangle = 9.0$ kcal mol^{-1}, which gives $\langle f_v\rangle = 0.26$. This estimate is consistent with other elimination processes, e.g., $\langle f_v\rangle \approx 0.2$ for elimination of H_2O from $CH_3C(O)OH$ or C_2H_5OH.[30,35]

5. Conclusions

Infrared chemiluminescence of the H_2O and HOD product molecules from the OH(OD) + H_2CO reaction has been used to measure their nascent vibrational energy distributions. The overall fractions for vibrational excitation were $\langle f_v(H_2O)\rangle = 0.56$ and $\langle f_v(HOD)\rangle = 0.54$ with a stretch-to-bend excitation ratio

of 1.9. The H_2O and HOD vibrational distributions closely resemble those from the HBr reaction. The room temperature reaction of OH with H_2CO has a 2-fold larger rate constant and a 5.7 kcal mol^{-1} larger exothermicity than for the $(CH_3)_2S$ reaction. However, the $\langle f_v(H_2O \text{ or HOD})\rangle$ and the stretch-to-bend excitation ratios are nearly the same. The vibrational distributions of water from H_2CO (and $(CH_3)_2S$ or HBr) do differ from those of saturated alkanes, like *n*-C_4H_{10} or cyclo-C_6H_{12}, which have much more inverted stretching distributions and 2-fold less bending excitation. These OH radical abstraction reactions release the expected energy to the newly formed bond, but the degree of bending excitation of H_2O or HOD depends on the molecular reagent. All evidence indicates that OH reacts with H_2CO by a direct abstraction mechanism in which the electron located in a p-orbital on the O atom attacks one of the H atoms of formaldehyde. The extremely weak emission (C═O stretch) observed from HCO demonstrates that the HCO product does not receive enough energy to cause dissociation. This low internal excitation of HCO is consistent with many other polyatomic reactions in which an H atom is directly abstracted.

In contrast to the OH + H_2CO reaction, the HCO radical reacts with OH radical by recombination to give vibrationally excited formic acid. The latter undergoes three-centered unimolecular elimination of H_2O before collisional stabilization at our pressures. The CO and H_2O vibrational distributions from the unimolecular decomposition of formic acid both decline with increasing vibrational energy.

The reactions of NO, NO_2, and H atoms with HCO at room temperature and 1 Torr pressure proceed mainly by recombination followed by unimolecular decomposition. The CO vibrational distribution from the H + HCO reaction is similar to those from the unimolecular decomposition of H_2CO that have been extensively studied by photoexcitation. This implies that the main pathway for H + HCO is recombination rather than abstraction.

The NO_2 + HCO reaction produces CO_2 molecules with bending excitation up to $v_2 = 13$ in H + NO + CO_2 channel plus strong CO emission from the HONO + CO channel. Comparison of the observed CO and CO_2 intensities shows that these two channels have approximately equal importance. A large fraction of the HONO molecules may undergo further dissociation to OH + NO, providing that the translational and rotational energy released to CO and HONO is negligible.

The HCO + NO reaction provides a strong source of HNO emission from the (200), (101), (110), and (100) bands. The experimental anharmonicity constants are $x_{11} = -116$ cm^{-1}, which is 3 cm^{-1} higher than calculated value, and $x_{12} = -69$ and $x_{13} = -27$ cm^{-1}, which are 25% lower than the calculated values.[33] The vibrational distribution with $\langle f_v(\text{HNO})\rangle \approx 0.26$ is consistent with three-centered unimolecular elimination from H(O)C−NO.

Acknowledgment. We acknowledge, with thanks, the assistance of Prof. Timothy J. Lee, who informed us about the calculations of the HNO spectroscopic constants, and Prof. Jonathan Tennyson, who provided data concerning water bands with high bending quantum numbers. We also thank Dr. L. B. Harding for a discussion of the H + HCO reaction and Dr. J. F. Hershberger for a preprint of ref 10. The work at Kansas State University was supported by the U.S. National Science Foundation (CHE-9505032).

References and Notes

(1) Atkinson, R.; Baulch, D. L.; Cox, R. A.; Hampson, Jr., R. F.; Kerr, J. A.; Troe, J. *J. Phys. Chem. Ref. Data* **1992**, *21*, 1125.

(2) Temps, F.; Wagner, H. Gg. *Ber. Bunsen-Ges. Phys. Chem.* **1984**, *88*, 415.

(3) Tsang, W.; Hampson, R. F. *J. Phys. Chem. Ref. Data* **1986**, *15*, 1087.

(4) Timonen, R. S.; Ratajczak, E.; Gutman, D. *J. Phys. Chem.* **1987**, *91*, 692.

(5) Horowitz, A.; Su, F.; Calvert, J. G. *Int. J. Chem. Kinet*. **1978**, *10*, 1099.

(6) He, Y.; Kolby, E.; Shumaker, P.; Lin, M. C. *Int. J. Chem. Kinet.* **1989**, *21*, 1015.

(7) Lin, C.-Y.; Wang, H.-T.; Lin, M. C.; Melius, C. F. *Int. J. Chem. Kinet*. **1990**, *22*, 455.

(8) Timonen, R. S.; Ratajczak, E.; Gutman, D. *J. Phys. Chem*. **1988**, *92*, 651.

(9) Guo, Y.; Smith, S. C.; Moore, C. B.; Melius, C. F. *J. Phys. Chem.* **1995**, *99*, 7473.

(10) Rim, K. T.; Hershberger, J. F. *J. Phys. Chem.* **1998**, *107*, 5899.

(11) Langford, A. O.; Moore, C. B. *J. Chem. Phys.* **1984**, *80*, 4211.

(12) Sarkisov, O. M.; Cheskis, S. G.; Nadtochenko, V. A.; Sviridenkov, E. A.; Vedeneev, V. I. *Arch. Combust*. **1984**, *4*, 111.

(13) Veyret, B.; Lesclaux, R. *J. Phys. Chem*. **1981**, *85*, 1918.

(14) Butkovskaya, N. I.; Setser, D. W. *J. Phys. Chem*. **1996**, *100*, 4853.

(15) Butkovskaya, N. I.; Setser, D. W. *J. Chem. Phys.* **1997**, *106*, 5028.

(16) Butkovskaya, N. I.; Setser, D. W. *J. Chem. Phys*. **1998**, *108*, 2434.

(17) Butkovskaya, N. I.; Setser, D. W. *J. Phys. Chem*. **1998**, *102*, 6395.

(18) (a) Holmes, B. E.; Setser, D. W. In *Physical Chemistry of Fast Reactions*; Smith, I. W. M., Ed.; Plenum: New York, 1980; Vol. 2, p 83; (b) Agrawalla, B. S.; Setser, D. W. In *Gas-Phase Chemiluminescence and Chemi-Ionization*; Fontijn, A., Ed.; Elsevier Science Publishers: Amsterdam, 1985; p 157; (c) Agrawalla, B. S.; Setser, D. W. *J. Phys. Chem.* **1986**, *90*, 2450.

(19) Becerra, R.; Carpenter, I. W.; Walsh, R. *J. Phys. Chem.* **1997**, *101*, 4185.

(20) Berkowitz, J.; Ellison, G. B.; Gutman, D. *J. Phys. Chem*. **1994**, *98*, 2744.

(21) Butkovskaya, N. I.; Muravyov, A. A.; Setser, D. W. *Chem. Phys. Lett*. **1997**, *266*, 223.

(22) (a) Wategaonakar, S. J.; Setser, D. W. *J. Chem. Phys*. **1989**, *90*, 251. (b) Rengarajan, R.; Setser, D. W.; DesMarteau, D. D. *J. Phys. Chem*. **1994**, *98*, 10568.

(23) Rothman, L. S.; Gamache, R. R.; Tipping, R. H.; Rinsland, C. P.; Smith, M. A. H.; Benner, D. C.; Devi, V. M.; Flaud, J.-M.; Camy-Payret, C.; Perrin, A.; Goldman, A.; Massie, S. T.; Brown, L. R.; Toth, R. A. The HITRAN Molecular Database: Editions of 1991 and 1992, *J. Quant. Spectrosc. Radiat. Transfer* **1992**, *48*, 469.

(24) Polyansky, O. L.; Zobov, N. F.; Vitti, S.; Tennyson, J.; Bernath, P. F.; Wallace, L. *Astrophys. J. Lett.* **1997**, *489*, L205.

(25) (a) *Molecular Constants of Inorganic Compounds*; Krasnov, K. S., Ed.; Chemistry: Leningrad, 1979. (b) Huber, K. P.; Herzberg, G. *Molecular Spectra and Molecular Structure. IV. Constants of Diatomic Molecules*; van Nostrand Reinhold Co.: New York, 1979.

(26) (a) Hure, J. M.; Roueff, E. *J. Mol. Spectrosc*. **1993**, *160*, 335. (b) Langhoff, S. R.; Bauschlicher, Jr., C. W. *J. Chem. Phys*. **1995**, *102*, 5220.

(27) Smith, I. W. M. *J. Chem. Soc., Faraday Trans.* **1997**, *93*, 3741.

(28) Braithwaite, M.; Smith, I. W. M. *J. Chem. Soc., Faraday Trans. 2* **1976**, *72*, 299.

(29) Werner, H.-J.; Bauer, C.; Rosmus, P.; Keller, H.-M.; Stumpf, M.; Schinke, R. *J. Chem. Phys*. **1995**, *102*, 3593.

(30) Butkovskaya, N. I.; Manke II, G.; Setser, D. W. *J. Phys. Chem*. **1995**, *99*, 1115.

(31) Suzuki, I. *J. Mol. Spectrosc*. **1968**, *25*, 479.

(32) Johns, J. W. C.; McKellar, A. R. W.; Weinberger, E. *Can. J. Phys.* **1983**, *61*, 1106.

(33) Dateo, C. E.; Lee, T. J.; Schwenke, D. W. *J. Chem. Phys*. **1994**, *101*, 5853.

(34) McKellar, A. R. W.; Burkholder, J. B.; Orlando, J. J.; Howard, C. J. *J. Mol. Spectrosc*. **1988**, *130*, 445.

(35) (a) Butkovskaya, N. I.; Setser, D. W. *J. Chem. Phys*. **1996**, *105*, 8064. (b) Butkovskaya, N. I.; Zhao, Y.; Setser, D. W. *J. Phys. Chem*. **1994**, *98*, 19779.

(36) Levine, R. D.; Bernstein, R. B. *Molecular Reaction Dynamics and Chemical Reactivity*; Oxford University Press: New York, 1987.

(37) Dane, C. B.; Lander, D. R.; Curl, R. F.; Tittel, F. K.; Guo, Y.; Ochsner, M. I. F.; Moore, C. B. *J. Chem. Phys*. **1988**, *88*, 2121.

(38) Dupuis, M.; Lester, Jr., W. A. *J. Chem. Phys*. **1984**, *81*, 847.

(39) Francisco, J. S. *J. Chem. Phys*. **1992**, *96*, 7597.

(40) McKee, M. L. *J. Phys. Chem*. **1993**, *97*, 10971.

(41) Sekusak, S.; Liedl, K. R.; Rode, B. M.; Sabljic, A. *J. Phys. Chem*. **1997**, *101*, 4245.

(42) Hu, W.-P.; Rossi, I.; Corchado, J. C.; Truhlar, D. G. *J. Phys. Chem*. **1997**, *101*, 6911.

(43) Nizamov, B.; Setser, D. W.; Wang, H.; Peslherbe, G. H.; Hase, W. L. *J. Chem. Phys*. **1996**, *105*, 9897.

(44) (a) Singleton, D. L.; Paraskevopoulos, G.; Irwin, R. S. *J. Phys. Chem*. **1990**, *94*, 695. (b) Irwin, R. S.; Singleton, D. L.; Paraskevopoulos, G.; McLaren, R. *Int. J. Chem. Kinet*. **1994**, *26*, 219.

(45) Francisco, J. S. *J. Chem. Phys*. **1992**, *96*, 1167.

(46) Goddar, J. D.; Yamaguchi, Y.; Schaefer III, H. F. *J. Chem. Phys*. **1992**, *96*, 1158.

(47) Zamir, E.; Levine, R. D. *Chem. Phys*. **1980**, *52*, 253.

(48) Harding, L. B.; Wagner, A. F. *Twenty-first Symposium (International) on Combustion*; The Combustion Institute: Pittsburgh, PA, 1986; p 721.

(49) Polik, W. F.; Guyer, D. R.; Moore, C. B. *J. Chem. Phys*. **1990**, *92*, 3453.

(50) Bamford, D. J.; Filseth, S. V.; Foltz, M. F.; Hepburn, J. W.; Moore, C. B. *J. Chem. Phys*. **1985**, *82*, 3032.

(51) Cheng, C.; Ho, P.; Moore, C. B.; Zughul, M. B. *J. Phys. Chem*. **1984**, *88*, 296.

(52) van Zee, R. D.; Pibel, C. D.; Butenhoff, T. J.; Moore, C. B. *J. Chem. Phys*. **1992**, *97*, 3235.

(53) van Zee, R. D.; Foltz, M. F.; Moore, C. B. *J. Chem. Phys*. **1993**, *99*, 1664.

(54) Chang, Y.-T.; Minichino, C.; Miller, W. H. *J. Chem. Phys*. **1992**, *96*, 4341.

(55) Chen, W.; Hase, W. L.; Schlegel, H. B. *Chem. Phys. Lett*. **1994**, *228*, 436.

(56) Tamagake, K.; Setser, D. W. In *State to State Chemistry*; Brooks, P. R., Hayes, E. F., Eds.; ACS Symposium Series, Vol. 56; American Chemical Society: Washington, DC, 1977.

(57) Beadle, P.; Dunn, M. R.; Jonathan, N. B. H.; Liddy, J. P.; Naylor, J. C.; Okuda, S. *J. Chem. Soc., Faraday Trans. 2* **1978**, *74*, 2158.

(58) Donaldson, D. J.; Sloan, J. J. *J. Chem. Phys*. **1985**, *82*, 1873.

(59) (a) Kim, E. H.; Bradforth, S. E.; Arnold, D. W.; Metz, R. B.; Neumark, D. M. *J. Chem. Phys*. **1995**, *103*, 7801. (b) Ayala, P. Y.; Schlegel, H. B. *J. Chem. Phys*. **1998**, *108*, 7560.